ELSEVIER

Ultramicroscopy 88 (2001) 127–138

ultramicroscopy

www.elsevier.nl/locate/ultramic

Investigations of the interference of surface plasmons on rough silver surface by scanning plasmon near-field microscope

V.N. Konopsky*, K.E. Kouyanov, N.N. Novikova

Institute of Spectroscopy, Russian Academy of Sciences, Moscow Region, Troitsk 142190, Russia

Received 11 June 2000; received in revised form 19 October 2000

Abstract

A scanning plasmon near-field microscope with gold and silver tips, operating in tapping mode of atomic force microscope is used to measure the distribution of the near-field intensity of surface plasmons on rough silver surfaces. Using the fast Fourier transformation of near-field images, it is shown that the distribution of the near-field intensity on the surface is the result of the interference between scattering plasmons and the initial plasmon beam. Multiple scattering effects such as backscattering enhancement of surface plasmons are also observed. It is shown that a nonuniformity in the registration of the scattered light leads to some artifacts in near-field images. Several registration modes of the light signal are considered and it is shown that recording the light signal at the second harmonic of the tapping frequency one can pick out the signal associated with an electromagnetic (em) resonance in a tip–surface (sphere–plane) structure. Possible implementations of this em resonance for studies of local permittivities and local nonlinear susceptibilities of intermediate media between the tip and surface with a subtip resolution are discussed.

PACS: 07.79.Fc; 61.16.Ch; 73.20.Mf

Keywords: Surface plasmons; Apertureless scanning near-field optical microscopy; Backscattering enhancement

1. Introduction

In a scanning near-field optical microscope (SNOM), a high-resolution optical image of a sample is obtained by scanning a subwavelength light source or detector close to the sample surface [1–4]. Aperture-type probes, e.g., aluminum-coated optical fibers tapered at their end have a typical aperture radius of 30–50 nm. In an apertureless scanning near-field microscope (aSNOM) a sharp tip of a scanning tunneling microscope (STM) or AFM is illuminated from the outside by an external light source and scatters the evanescent field which is then far-field detected [5]. The lateral resolution of aSNOM is determined by the tip size and reaches the value of 17–20 nm [6,7].

A scanning plasmon near-field microscope (SPNM) [8–14] may be considered as an aSNOM in which a traveling surface plasmon field on the silver surface is used as an external excitation source of aSNOM tip. Using gold- and silver-

*Corresponding author. Fax: +7-095-334-08-86.
E-mail address: konopsky@isan.troitsk.ru (V.N. Konopsky).

0304-3991/00/$ - see front matter
PII: S0304-3991(00)00131-5

coated cantilever tips, it is possible to excite an em resonance in the tip–surface (sphere–plane) structure and reach a resolution less than a tip radius [15]. In this paper we use this approach to study the behavior of surface plasmons on rough silver surfaces.

The plan of this paper is as follows: in Section 2 we describe our experimental setup and different registration modes of the light signal. In Section 3 we present and discuss our experimental results: a distance-dependent variation of the light signal, the distribution of the near-field intensity of the surface plasmons on rough silver surface and FFT of this intensity; we consider artifacts in near-field images due to a nonuniformity in the registration of the scattered light and finally describe multiple scattering effects. In Section 4 we give the conclusions.

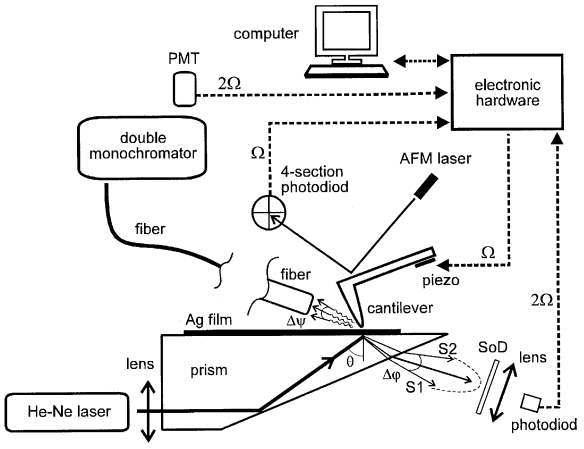

Fig. 1. Schematic of the experimental setup: PMT – photomultiplier tube, SoD – set of diaphragms; scattered rays S1–S2 and angle $\Delta\varphi$ between them lie in the plane which is perpendicular to the plane of the figure.

2. Experimental setup

Our experimental setup is schematically shown in Fig. 1. A beam of a cw He–Ne laser ($\lambda = 632.8$ nm, $I \simeq 1$ mW) incident on a silver film at a defined angle θ_0 of total internal reflection excites the surface plasmons at the silver–air interface (the usual Kretschmann configuration). Silver films of thickness 500 Å were prepared by thermal evaporation of Ag on the base of the quartz prism at the pressure 5×10^{-6} torr at a room temperature. The deposition rate of silver was about 5 Å/s. The thickness of silver films was measured using a quartz crystal monitor disposed near the base of the quartz prism. For studies of multiple scattering effects we need silver films with large pointlike surface irregularities, and even with several closely spaced irregularities (to investigate a backscattering enhancement effect). For this purpose we proceed as follows: after completion of a work with a silver film and removing one from the prism base by nitric acid we evaporate the next film on the prism base without preliminary polishing and/or fire polishing of the prism base (as is done if smooth film is desirable). After two–four such turns we obtain the films which may be used in studies of multiple scattering effects.

The excitation of the SPs is recognized as a minimum in the reflected laser intensity and can be understood as destructive interference between the light reflected from the silver–air and the silver–quartz interfaces [16]. A commercial scanning probe microscope "Solver P-47" of "NT-MDT" firm [17] with gold- and silver-coated silicon cantilevers has been used in common AFM mode (a bend of the cantilever is held constant by AFM feedback during scan) and in tapping mode of AFM (an amplitude of the cantilever vibration is held constant by AFM feedback during scan).

Several registration modes of the light signal are used in our setup.

(1) "*Internal reflection registration mode*" – is the registration of the intensity variation of the reflected light beam. (scattered light rays (S1–S2) are removed by the set of diaphragms – SoD). This registration mode is the one that was used in the works [8,9].

(2) "*Internal scattering registration mode*" – is the registration of the intensity of the conical light radiation arisen from an elastic scattering of the surface plasmons in the angle $\Delta\varphi$ between rays S1 and S2 (reflected light beam is removed by the set of diaphragms – SoD). S1 and S2 are the extreme left and extreme right rays of the conical scattered light radiation that is collected by the lens on the

photodiode. This registration mode is similar to the one that was used in the works [10–13], but in these works the overall conical scattered light radiation was collected by a cylindrical mirror (i.e. $\Delta\varphi = 2\pi$ in these works; in our case $\Delta\varphi \simeq 23^\circ$).

(3) "*External scattering registration mode*" – is the registration of the plasmon–photon scattering using the multimode fiber with diameter 300 μm and numerical aperture ≈ 0.4 placed in the immediate vicinity (0.5 mm) of the cantilever tip. An undesirable scattered light from an AFM laser diode ($\lambda \simeq 670$ nm) has been removed by a double monochromator. The light signal has been detected by a photo-multiplier tube (PMT) placed on the exit of the double monochromator.

In each above-mentioned registration modes the light signal can be recorded:

(a) *without modulation*: that is, AFM operates in the common mode and the light signal detected at zero frequency;

(b) *at the first harmonic of the cantilever vibration*: that is, AFM operates in the tapping mode and the light signal detected at a frequency Ω of a cantilever vibration;

(c) *at the second harmonic of the cantilever vibration*: that is, AFM operates in the tapping mode and the light signal detected at a frequency 2Ω.

A typical value of the resonant frequency of gold- and silver-coated cantilevers in our setup was $\Omega \approx 40$ kHz. An amplitude of the cantilever vibration was about 150 nm, and it was kept constant by AFM feedback during the scan.

3. Experimental results and discussion

3.1. Distance-dependent variation of the light signal and the em resonance in a tip–surface structure

To understand the advantages of the light registration at the second harmonic of the tip–surface distance modulation one must consider the variation of the light signal while the tip–sample distance is varied. The distance-dependent intensity of the light signal in the "external scattering registration mode" is presented in Fig. 2. A gold-coated silicon tip with $R \simeq 190$ nm is used to

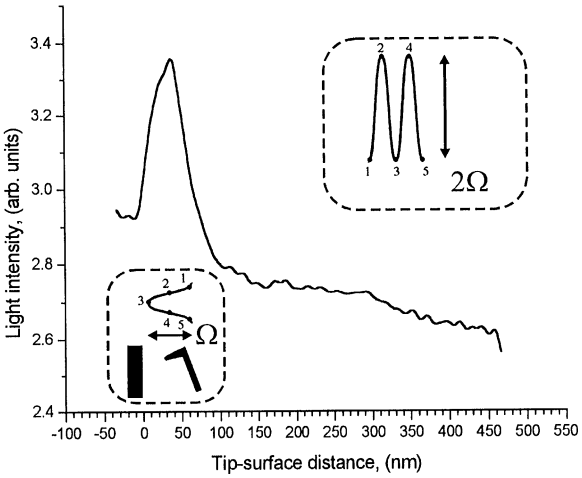

Fig. 2. The distance-dependent intensity of the light signal in "external scattering registration mode". On insets in dashed-line frames the mechanism of the 2Ω frequency generation at the tip–surface distance modulation by Ω frequency is illustrated.

obtained this dependence. One can see that light intensity decreases during the tip withdrawal from the surface, but some maximum ("bump") takes place at the curve at $x = 35$ nm.

Similar "bumps" on distance-dependent intensity curves were also detected by other authors in different registration modes of SPNM. See, for example, Refs. [8,14] ("internal reflection registration mode") and also [10] ("internal scattering registration mode"), but we have found that in the "external scattering registration mode" this maximum is more pronounced. A detailed discussion about the origin of this maximum has been done elsewhere [15]. Here we present only our main conclusions. We believe that this maximum takes place due to the em resonance in the tip–surface (sphere–plane) structure. The em resonance in the sphere–plane structure was thoroughly studied in the early 1980s in the context of a light emission from small particle tunnel junctions [18,19], and in the context of surface-enhanced Raman scattering [20]. In visible region this em resonance is of greater intensity when the tip and the surface are noble metals. The resonances in the sphere–plane structure at $d \ll R$ are often called "gap modes". Eigen frequencies of these modes may be determined from the next approximated analytical

expression [21]

$$\frac{\varepsilon_0}{\varepsilon_1'(\omega)}+\frac{\varepsilon_0}{\varepsilon_2'(\omega)}=-\left(n+\tfrac{1}{2}\right)\sqrt{\frac{2d}{R}},\quad n=0,1,2,\ldots\ , \tag{1}$$

where $\varepsilon_2'(\omega)$ and $\varepsilon_1'(\omega)$ are the real parts of the permittivities of the sphere and the plane. In our configuration (see Fig. 3) $\varepsilon_2'(\omega)$ and $\varepsilon_1'(\omega)$ are the real parts of the permittivities of the tip and the surface, R is the radius of curvature of the tip and d is the distance between the tip and the surface. Therefore, if we excite the gap between the needle and the surface by an em radiation with a fixed frequency (e.g. by He–Ne laser) the em resonance in this sphere–plane structure occurs at the next "resonance" distance between the tip and the surface

$$d_{\mathrm{res}}=2R\left[\frac{\varepsilon_0}{\varepsilon_1'(\omega_{\mathrm{HeNe}})}+\frac{\varepsilon_0}{\varepsilon_2'(\omega_{\mathrm{HeNe}})}\right]^2 \tag{2}$$

(hereinafter, we shall consider "gap mode" with $n=0$). In other words, an "effective" dipole moment of the sphere–plane structure has a maximum amplitude at $d=d_{\mathrm{res}}$, and it decreases when the tip approaches the surface at the distance $d<d_{\mathrm{res}}$ and moves away from the surface at the distance $d>d_{\mathrm{res}}$. For good agreement with observed value of $d_{\mathrm{res}}\simeq 35$ nm it is necessary that "effective" permittivity of intermediate layers (chiefly silver sulfide tarnished layer [22]: $\varepsilon'_{\mathrm{Ag_2S}}=8.7$ and adsorbed water: $\varepsilon'_{\mathrm{H_2O}}=1.8$) between the tip and the silver surface was about $\varepsilon_0\approx 2$.

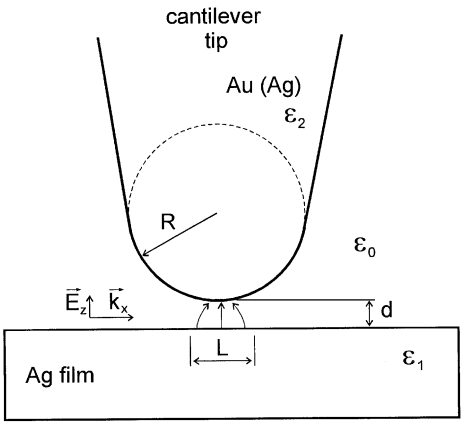

Fig. 3. The tip–surface structure and the light field localization beneath the tip.

The important characteristic feature of the sphere–plane em resonance is the lateral dimension L of the em field localization between the sphere and the plane. It is approximately equal to [18,19,21]

$$L\approx\sqrt{2dR}. \tag{3}$$

Therefore, at $d\ll R$ this dimension is less than the tip radius ($L<R$). As a result the huge increase of the light intensity under sphere takes place [19,20].

If we modulate the tip–surface distance at a frequency Ω, then we can pick out the signal associated with the sphere–plane resonance by detecting a light signal at the frequency 2Ω. Returning to Fig. 2 one can see on insets in dashed-line frames the elucidation of the mechanism of the 2Ω frequency generation at the tip–surface distance modulation by Ω frequency: one may consider how the light intensity changes when the tip makes one complete cycle of vibration. Points 1–5 on the intensity variation curve correspond to the points 1–5 on the tip position curve. It is seen from these curves that the light intensity turns twice while the tip makes one turn.

The registration of the light signal at the second harmonic of the distance modulation (that is, in fact, the registration of the em resonance signal) opens up several new possibilities for studies of surface with nanometer resolution. The most straightforward of them is the use of huge field enhancement of the em field under tip for registration of the nonlinear effects such as Raman scattering or second harmonic generation with a resolution about L. For example, the registration of the second harmonic will provide the information about nonlinear susceptibilities of the [tip–intermediate layer-surface] structure with a resolution even better than L. Another possible implementation of the tip–surface em resonance opens up if one detects (in each point of the surface) the *spacing* between the tip and the surface at which the em resonance occurs. So this distance strongly depends on the intermediate media permittivity ($d_{\mathrm{res}}\sim\varepsilon_0^2$) such a registration will provide the information about ε_0 with a subtip

resolution. For example, molecules with a resonance line at the laser frequency deposited on the surface may be visualized in such a manner.

3.2. Distribution of the near-field intensity of the surface plasmons on rough silver surface: interference between scattering plasmons and the initial plasmon beam

Fig. 4b illustrates the distribution of the near-field intensity of the surface plasmon field on a silver surface (direction of the initial surface plasmon beam designated by the arrows). Scan size is 15 800 nm × 16 800 nm. The optical signal was recorded at 2Ω frequency in the "internal reflection registration mode" (i.e. 1c mode in our notation, see Section 2). A gold-coated silicon tip with $R \simeq 190$ nm is used to obtain this image. From mathematical data processing of the topography of this part of the surface (Fig. 4a) we obtain the root-mean-square height of the surface roughness $\delta = \langle(\Delta z)^2\rangle^{1/2} \simeq 3.8$ nm.

From comparison of the surface topography (Fig. 4a) and the near-field image (Fig. 4b) one can make the next conclusions:

(a) prominent surface hillocks, such as the hillocks 1–5, appear in the near-field image as the white spots 1–5 (reasons why hillocks have negative contrast have been given elsewhere [15])

(b) other prominent surface features, such as the ditch 6 in the up-right corner of Fig. 4a, also lead to a expected interference pattern in the vicinity of these features, but

(c) apart from that, some additional ripples and fringes, which cannot be associated with any particular surface features, are appearing on the near-field images.

The similar near-field pictures have been observed by other authors using SPNM (see, for instance [8,10–12]) and SNOM [23–25]. But to our knowledge, the reasons for appearance of such "cluster structure" of the em field which are not associated with any particular features in the surface topography have not been clearly illuminated. To attain such an understanding one must perform the Fourier transformation (FFT) of the near-field image. In Fig. 4d one can see a distinct circle in the FFT of the near-field image (the second circle arises because of inherent feature of Fourier transformations: a FFT image is symmetric respective to the origin of the coordinates). The explanation of the appearance of such a circle in the FFT image is given in Fig. 4c. The initial surface plasmon beam is scattered by surface irregularities and interference between the initial surface plasmon beam and scattering plasmons takes place. At elastic scattering the wavevector of the initial plasmon $\boldsymbol{k}_{\mathrm{pl}}$ changes its direction, but its magnitude remains the same ($|\boldsymbol{k}_{\mathrm{pl}}| = |\boldsymbol{k}_{\mathrm{sc}}|$). The distribution of the SP near-field intensity on the surface is $I_{\mathrm{pl}} + I_{\mathrm{sc}} + 2\sqrt{I_{\mathrm{pl}} I_{\mathrm{sc}}}\cos((\boldsymbol{k}_{\mathrm{pl}} - \boldsymbol{k}_{\mathrm{sc}})\boldsymbol{r})$. So the "vectors of the interference gratings" $\boldsymbol{K}_{\mathrm{int}} = \boldsymbol{k}_{\mathrm{pl}} - \boldsymbol{k}_{\mathrm{sc}}$ are distributed so that their ends lie on the circle with radius equals $|\boldsymbol{k}_{\mathrm{pl}}|$. One can see from the FFT image that forward scattering (small $\boldsymbol{K}_{\mathrm{int}}$) is of the greatest intensity. In the case when effects of the multiple scattering (see Section 3.4) are negligible the intensity along this circle must be proportional to the roughness function $\delta h(\boldsymbol{g}_{\mathrm{r}})$ (i.e. FFT of the surface topography). The angular dependence of surface plasmon scattering by surface irregularities is of great concern, for example, in studies of a laser damage of metal mirrors. The surface plasmons play a crucial role in such a damage [28] and elimination of the surface plasmons caused by the surface roughness is of considerable importance for increasing the laser damage threshold of metal mirrors [29].

3.3. Artifacts in near-field images due to nonuniformity at the registration of the scattered light

In some works with SPNM, operating in the "internal scattering registration mode", the large-scale interference pattern is silhouetted against of the "cluster structure" background (see, e.g. Ref. [11]). We believe that this effect occurs due to a nonuniformity in the registration of the scattered light in this mode. To prove this assumption we shut off not only the reflected beam, but also the scattered light rays between the reflection beam and S2 beam in our setup (see Fig. 1). That is, only scattered light rays between the reflected beam and S1 beam have been used in the "internal scattering registration mode". The results are presented in Fig. 5 (scan size is 7200 × 7200 nm). A gold-

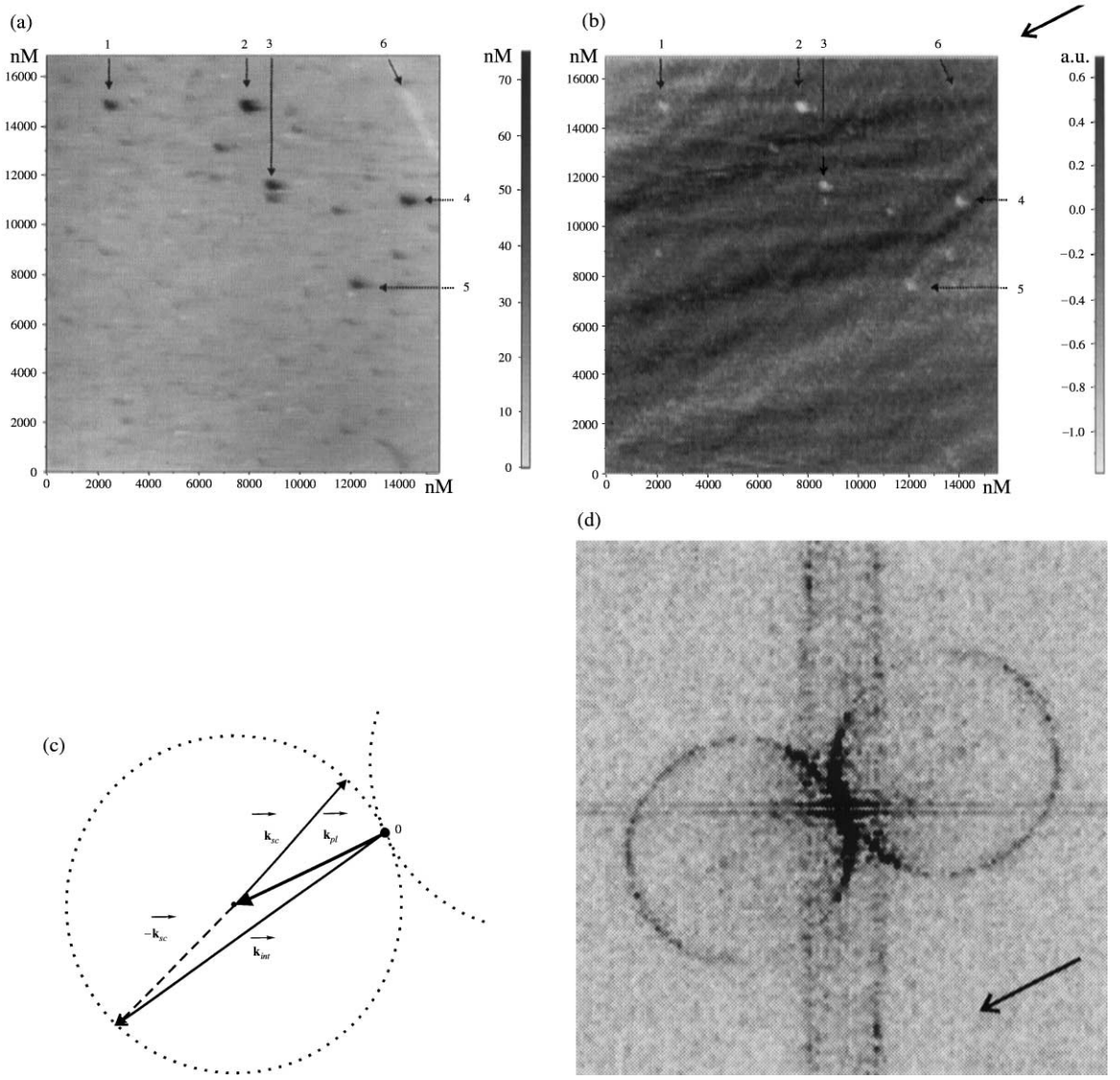

Fig. 4. AFM (a) and SPNM (b) images of the silver surface (scan size is 15 800 nm × 16 800 nm). (d) is FFT of SPNM image (the arrow length on FFT image corresponds the surface plasmon wavevector length $|\boldsymbol{k}_{\mathrm{pl}}|$) and (c) is the schematic of the surface plasmon interference. Dotted arrows on (a) and (b) images pointed out prominent surface features (see text).

coated silicon tip with $R \simeq 190$ nm is used to obtain this image. One can see that a large-scale interference pattern appears in near-field images recorded by different methods: Fig. 5c – *without modulation*, Fig. 5d – *at the first harmonic of the cantilever vibration*, Fig. 5e – *at the second harmonic of the cantilever vibration*. In the FFT image (5f) of Fig. 5e a pronounced point, which corresponds to this large-scale interference pattern, appears (the second point is symmetric to the first one with respect to the origin of the coordinates). The reasons for this are as follows: inasmuch as the forward scattering is of the greatest intensity, an appearance of a particular "preferable" direction in the registration system (i.e. nonuniformity) leads to the enhancement of

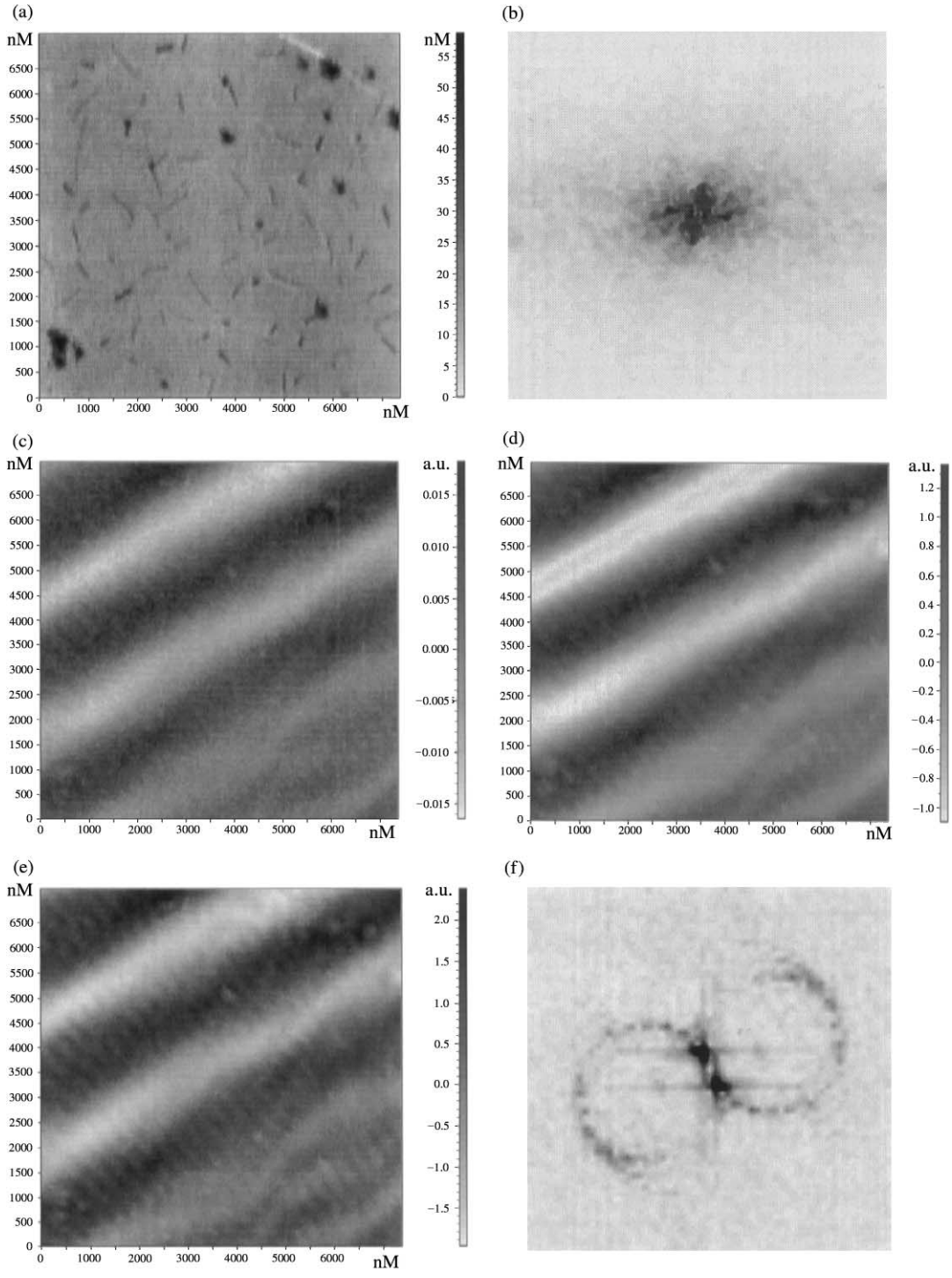

Fig. 5. Topography (a) and FFT of the topography (b) of the silver surface (scan size is 7200 nm × 7200 nm), (c)–(e) are the near-field images recorded: (c) – without modulation, (d) – at the first harmonic of the cantilever vibration, (e) – at the second harmonic of the cantilever vibration in the ''internal scattering registration mode'' with nonuniform registration of the light signal. (f) is the FFT image of the (e) image.

the contribution from plasmons that scattered in this particular direction. The period of this interference pattern is

$$\Lambda = \frac{\lambda}{2\sin(\Delta\varphi/2)}, \tag{4}$$

where $\Delta\varphi$ is the mean angle between the direction of the scattered light rays and the direction of the initial plasmon beam.

From Fig. 5 one can also see that near-field images recorded at the second harmonic of the cantilever vibration have the best resolution.

3.4. Multiple scattering effects

3.4.1. SP scattering between the tip and surface irregularities

In the works done with tapered fibers in near-field microscopy (see Refs. [23–27] and bibliography mentioned therein) the use of a dielectric tip assures that the interaction between the tip and SPs is negligible and the presence of the dielectric tip does not influence the near-field images. In our experimental arrangement, in fact, we use a large dipole moment of the tip–surface structure as a local probe of the SP field distribution. On the flat surface, where the dipole p of the surface–tip structure is the only prominent scattered center, intensity of SP scattering in the "internal scattering mode" and a value of the SP extinction (scattering plus absorbtion) induced by this probe dipole in the "internal reflection mode" are proportional to SP intensity in the absence of the tip ($p = \alpha E_{\mathrm{sp}}$, $I_{\mathrm{sc}} \sim \ddot{p}^2 \sim |E_{\mathrm{sp}}|^2$, where α – the polarizability of the tip–surface structure).

The situation changes when other effective scattering centers of SPs are present on the surface. In this case the SP scattered by the tip may be rescattered by such a scattering center and return to the tip. That is, the SP field at the tip position becomes not the same as in the absence of the tip. This type of effect of multiple scattering becomes important for very large surface hillocks – when a cross-section of surface plasmon scattering of a large hillock and the one of the tip become comparable in magnitude. In this case typical V-shaped figures near large point-like hillocks occur in the SPNM image. The detailed description of such effects can be found in Ref. [13]. We have found that in our setup these effects became well defined at the surface hillock height $h > 100$ nm. But even in this case the circle in the FFT of the near-field images takes place, but the intensity distribution along the circle changes. Fig. 6 is the illustration of this effect. Scan size is 25 000 nm × 20 000 nm, the root-mean-square height of the surface roughness $\delta = \langle(\Delta z)^2\rangle^{1/2} \simeq 13.2$ nm. The near-field image is recorded in "internal reflection registration mode" at the second harmonic of the cantilever vibration. A silver-coated silicon tip with $R \simeq 150$ nm is used to obtained this image.

3.4.2. Backscattering enhancement effect

Another effect of multiple scattering is a backscattering enhancement of surface plasmons on a random surface. For a detailed consideration of this subject one can see the theoretical works [30–33], and experimental work [34] in this area of exploration (although in the above-mentioned works a significantly different experimental procedure was considered). We shall confine our account to a purely qualitative discussion of the problem. The initial plasmon wave scatters from a point on the rough surface and reaches another point on the surface where it is scattered once again. The time-reversed version of this process will also occur, in which the initial plasmon wave interacts with the second point and then couples to an outgoing wave at the first point. These two sequences produce diffuse scattering contributions that interfere constructively in the opposite direction to the initial plasmon wave direction. Further, this argument holds for all pairs of points on rough surface and, upon averaging, a narrow backscattering peak is produced. Therefore, $\boldsymbol{k}_{2\mathrm{sc}} = -\boldsymbol{k}_{\mathrm{pl}}$ and in FFT image at $\boldsymbol{K}_{\mathrm{int}} \equiv 2\boldsymbol{k}_{\mathrm{pl}}$ a local maximum associated with the backscattering enhancement will occur.

The effect of the backscattering enhancement is easy to record on such a part of a surface where several closely spaced prominent (not necessarily very large) hillocks are present. The example is shown in Fig. 7. Scan size is 18 000 nm × 18 000 nm, the root-mean-square

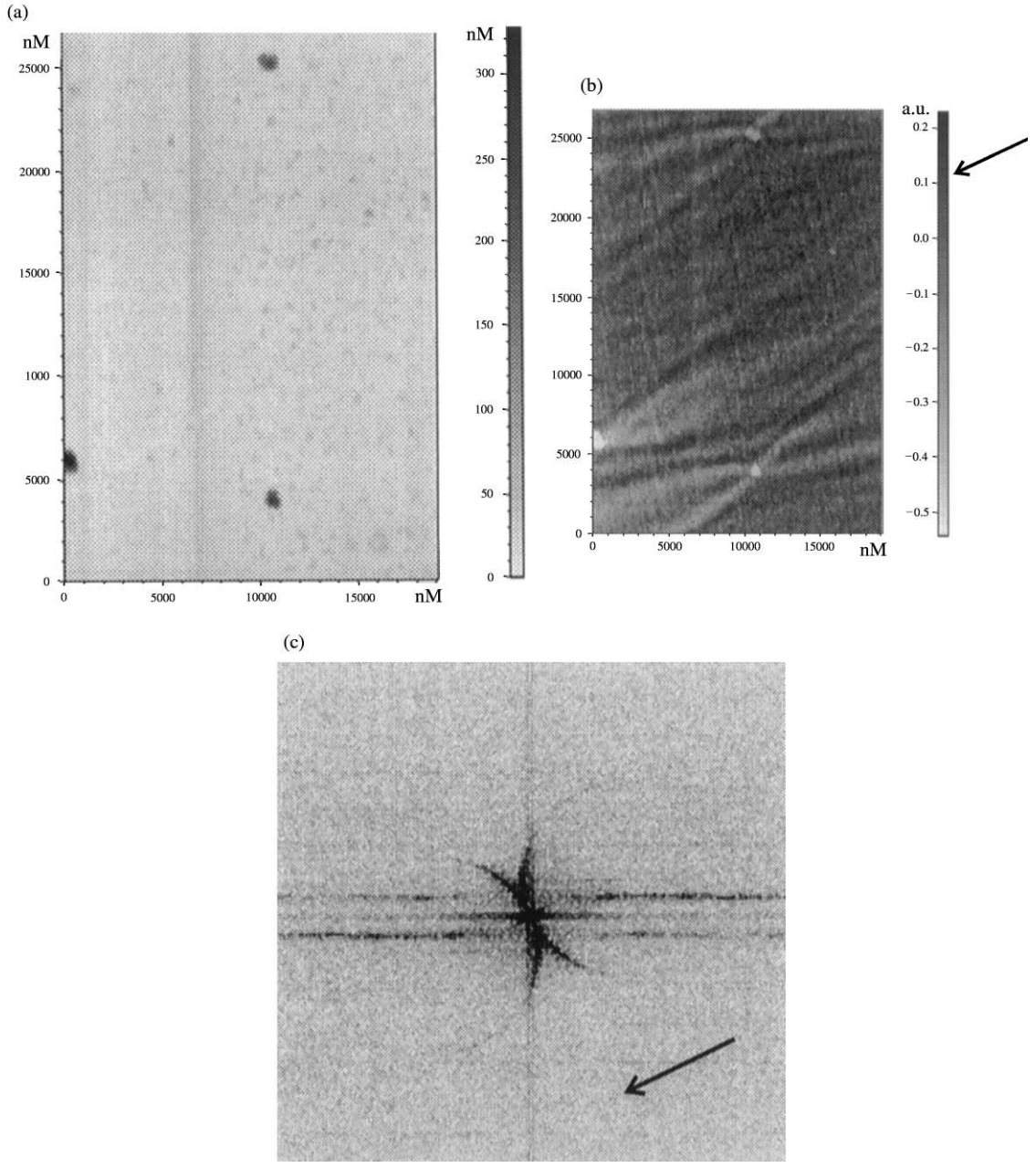

Fig. 6. Effects of the SP scattering between the tip and large hillocks: topography (a), the near-field image of the surface (b) and FFT of the near-field image (c) (the arrow length on FFT image corresponds to the surface plasmon wavevector length $|\boldsymbol{k}_{\mathrm{pl}}|$). Scan size is 25 000 nm × 20 000 nm.

height of the surface roughness $\delta = \langle(\Delta z)^2\rangle^{1/2} \simeq 7.2$ nm. The optical signal is recorded in "internal reflection registration mode" at the first harmonic of the cantilever vibration. A silver-coated silicon tip with $R \simeq 150$ nm is used to obtained this image. The maximum arises from the backscattering enhancement denoted by a dotted arrow on the FFT image (Fig. 7c).

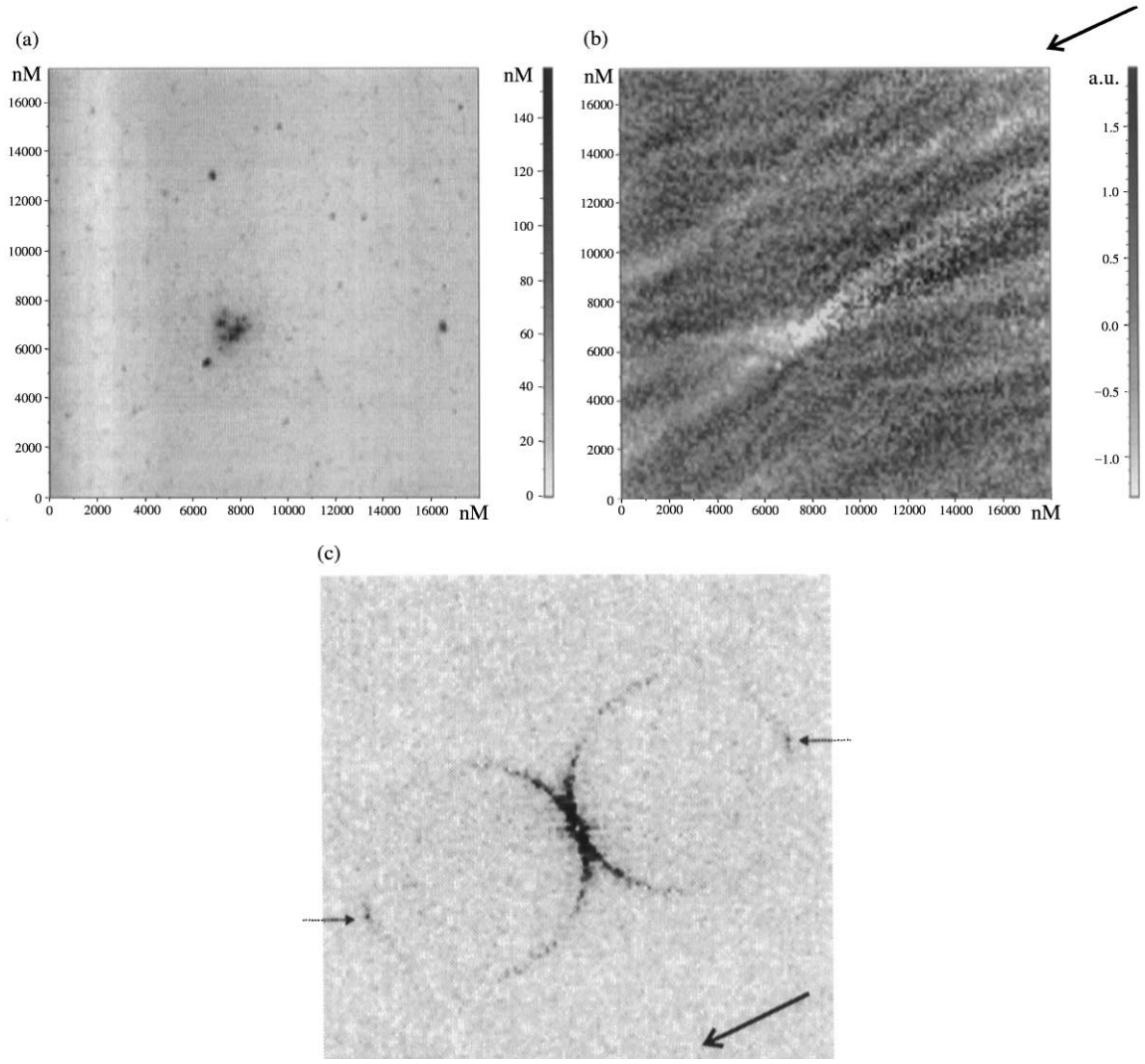

Fig. 7. The backscattering enhancement effect: topography (a), the near-field image (b) of the surface and FFT of the near-field image (c) (the arrow length on FFT image corresponds to the surface plasmon wavevector length $|\boldsymbol{k}_{\mathrm{pl}}|$). Dotted arrows on the FFT image points out the maximum which arises from the backscattering enhancement. Scan size is 18 000 nm × 18 000 nm.

It may be noted that authors of the works [23,24] tried to observe the effect of the backscattering enhancement by looking for the interference fringes with $\lambda_{\mathrm{sp}}/2$ period in the direction of the initial SP beam. It has been pointed out [23,24] that desirable interference pattern is difficult to observe due to the presence of other interference patterns related to different scattered SPs.

We hope that the present work demonstrates that the Fourier transformation of the near-field images is a simple and powerful tool for studies of such effects.

4. Conclusions

In this paper, we have used a scanning plasmon near-field microscope, operating in tapping mode of AFM, to measure the distribution of the near-field intensity of surface plasmons on rough silver

surfaces. Using the fast Fourier transformation (FFT) of near-field images it has been shown that distribution of the near-field intensity on the surface is the result of the interference between scattering plasmons and the initial plasmon beam. Multiple scattering effects such as backscattering enhancement of the surface plasmons have also been observed using FFT of near-field intensity. We have shown that a nonuniformity in the registration of the scattered light leads to certain artifacts in near-field images.

We have used gold and silver-coated cantilevers to enhance an electromagnetic resonance in a tip–surface (sphere–plane) structure. We have recorded the optical signal at the second harmonic of tapping frequency to pick out the signal associated with the sphere–plane em resonance. The spatial resolution of the light signal at the tip–surface em resonance is determined by the dimension of the light field localization beneath the tip and it may be less than the tip radius. Possible implementations of this em resonance for studies of local permittivities and local nonlinear susceptibilities of intermediate media between the tip and surface with a subtip resolution have been discussed.

In closing, it may be said that proposed method of investigation of the surface plasmon distribution on the rough surface may be improved in several aspects. One of them is as follows: to improve the resolution of the FFT images one must perform the large-size scans (100 μm × 100 μm or more) of the surface. In this case one can reach the ultimate FFT resolution $\delta k/k \sim \lambda/l_{sp}$, where l_{sp} – mean free path of surface plasmons. Several interesting fine effects may be observed in this case, for example, the energy band gap of the surface plasmon curve due to the interaction of the initial plasmon beam ($\boldsymbol{k}_{pl}$) with spatial frequency component of the surface roughness $\boldsymbol{g}_r \simeq 2\boldsymbol{k}_{pl}$, when an amplitude of this component is not very small (for more details, see Ref. [35,36] and references therein). On several FFT images we have observed the splitting of the circle at $\boldsymbol{K}_{int} \simeq 2\boldsymbol{k}_{pl}$ (a hint on such a splitting may be found in Fig. 4d). But the largest possible scan size in our setup is 25 μm × 25 μm and the improvement of the FFT resolution is necessary to study such effects.

Acknowledgements

Authors thank Y.E. Petrov for help with the silver coating of cantilevers and prisms and A.M. Lifshits for supply of optical fibers. The present research was supported by RFFI grant and by programs "Fundamental Spectroscopy" and "Fundamental Metrology" of Russian Ministry of Science.

References

[1] E.H. Synge, Philos. Mag. 6 (1928) 356.
[2] E.A. Ash, G. Nicholls, Nature 237 (1972) 510.
[3] D.W. Pohl, W. Denk, M. Lanz, Appl. Phys. Lett. 44 (1984) 651.
[4] E. Betzig, J.K. Trautman, T.D. Harris, J.S. Weiner, R.L. Kostelak, Science 251 (1991) 1468.
[5] F. Zenhausern, M.P. O'Boyle, H.K. Wickramasinghe, Appl. Phys. Lett. 65 (1994) 1623.
[6] A. Lahrech, R. Bachelot, P. Gleyzes, A.C. Boccara, Opt. Lett. 21 (1996) 1315.
[7] R. Bachelot, P. Gleyzes, A.C. Boccara, Appl. Opt. 36 (1997) 2160.
[8] M. Specht, J.D. Pedarnig, W.M. Heckl, T.W. Hänsh, Phys. Rev. Lett. 68 (1992) 476.
[9] J.D. Pedarnig, M. Specht, W.M. Heckl, T.W. Hänsh, Appl. Phys. A 55 (1992) 476.
[10] Y-K. Kim, P.M. Lundqist, J.A. Helfrich, J.M. Mikrut, G.K. Wong, P.R. Auvil, J.B. Ketterson, Appl. Phys. Lett. 66 (1995) 3407.
[11] Y-K. Kim, J.B. Ketterson, D.J. Morgan, Opt. Lett. 21 (1996) 165.
[12] Y-K. Kim, P.R. Auvil, J.B. Ketterson, Appl. Opt. 36 (1997) 841.
[13] P.R. Auvil, J.B. Ketterson, Y-K. Kim, A. Kryukov, Appl. Opt. 37 (1998) 8448.
[14] J. Boneberg, M. Ochmann, H.-J. Münzer, P. Leiderer, Ultramicroscopy 71 (1998) 345.
[15] V.N. Konopsky, Opt. Commun. 185 (2000) 83.
[16] H. Raether, Surface Plasmons, Springer Tracts in Modern Physics, Vol. 111, Springer, Berlin, 1988.
[17] http://www.ntmdt.ru
[18] R.W. Rendell, D.J. Scalapino, B. Mühlschlegel, Phys. Rev. Lett. 41 (1978) 1746.
[19] R.W. Rendell, D.J. Scalapino, Phys. Rev. B 24 (1981) 3276.
[20] P.K. Aravind, H. Metiu, Surf. Sci. 124 (1983) 506.
[21] A.G. Mal'shukov, Phys. Rep. 194 (1990) 343.

[22] J.M. Bennett, J.L. Stanford, E.J. Ashley, J. Opt. Soc. Am. 60 (1970) 224.
[23] S.I. Bozhevolnyi, Phys. Rev. B 54 (1996) 8177.
[24] S.I. Bozhevolnyi, A.V. Zayats, B. Vohnsen, in: M. Nieto-Vesperinas, N. Garcia (Eds.), Optics at the Nanometer Scale, Kluwer, Dordrecht, 1996, p. 163.
[25] J.R. Krenn, R. Wolf, A. Leitner, F.R. Aussengg, Opt. Commun. 137 (1997) 46.
[26] I.I. Smolyaninov, D.L. Mazzoni, J. Mait, C.C. Davis, Phys. Rev. B 56 (1997) 1601.
[27] S.I. Bozhevolnyi, B. Vohnsen, E.A. Bozhevolnaya, Opt. Commun. 172 (1999) 171.
[28] A.E. Siegman, P.M. Fauchet, IEEE J. Quantum Electron. QE-22 (1986) 1384.
[29] V.N. Konopsky, Opt. Laser Technol. 32 (2000) 15.
[30] A.R. McGurn, A.A. Maradudin, V. Celli, Phys. Rev. B 31 (1985) 4866.
[31] V. Celli, A.A. Maradudin, A.M. Marvin, A.R. McGurn, J. Opt. Soc. Am. A 2 (1985) 2225.
[32] A.R. McGurn, A.A. Maradudin, J. Opt. Soc. Am. B 4 (1987) 910.
[33] A.A. Maradudin, E.R. Méndez, Appl. Opt. 32 (1993) 3335.
[34] C.S. West, K.A. O'Donnell, J. Opt. Soc. Am. A 12 (1995) 390.
[35] A.A Maradudin, in: V.M. Agranovich, D.L. Mills (Eds.), Surface Polaritons, North-Holland, Amsterdam, 1982.
[36] W.L. Barnes, T.M. Preist, S.C. Kitson, J.R. Sambles, Phys. Rev. B 54 (1996) 6227.